

# Improvement in Muon Track Reconstruction with Robust Statistics

M. G. Aartsen<sup>2</sup>, R. Abbasi<sup>27</sup>, Y. Abdou<sup>22</sup>, M. Ackermann<sup>41</sup>, J. Adams<sup>15</sup>,  
J. A. Aguilar<sup>21</sup>, M. Ahlers<sup>27</sup>, D. Altmann<sup>9</sup>, J. Auffenberg<sup>27</sup>, X. Bai<sup>31,1</sup>,  
M. Baker<sup>27</sup>, S. W. Barwick<sup>23</sup>, V. Baum<sup>28</sup>, R. Bay<sup>7</sup>, J. J. Beatty<sup>17,18</sup>,  
S. Bechet<sup>12</sup>, J. Becker Tjus<sup>10</sup>, K.-H. Becker<sup>40</sup>, M. Bell<sup>38</sup>,  
M. L. Benabderrahmane<sup>41</sup>, S. BenZvi<sup>27</sup>, J. Berdermann<sup>41</sup>, P. Berghaus<sup>41</sup>,  
D. Berley<sup>16</sup>, E. Bernardini<sup>41</sup>, A. Bernhard<sup>30</sup>, D. Bertrand<sup>12</sup>, D. Z. Besson<sup>25</sup>,  
G. Binder<sup>8,7</sup>, D. Bindig<sup>40</sup>, M. Bissok<sup>1</sup>, E. Blaufuss<sup>16</sup>, J. Blumenthal<sup>1</sup>,  
D. J. Boersma<sup>39</sup>, S. Bohaichuk<sup>20</sup>, C. Boehm<sup>34</sup>, D. Bose<sup>13</sup>, S. Böser<sup>11</sup>,  
O. Botner<sup>39</sup>, L. Brayeur<sup>13</sup>, H.-P. Bretz<sup>41</sup>, A. M. Brown<sup>15</sup>, R. Bruijn<sup>24</sup>,  
J. Brunner<sup>41</sup>, M. Carson<sup>22</sup>, J. Casey<sup>5</sup>, M. Casier<sup>13</sup>, D. Chirkin<sup>27</sup>,  
A. Christov<sup>21</sup>, B. Christy<sup>16</sup>, K. Clark<sup>38</sup>, F. Clevermann<sup>19</sup>, S. Coenders<sup>1</sup>,  
S. Cohen<sup>24</sup>, D. F. Cowen<sup>38,37</sup>, A. H. Cruz Silva<sup>41</sup>, M. Danninger<sup>34</sup>,  
J. Daughhetee<sup>5</sup>, J. C. Davis<sup>17</sup>, C. De Clercq<sup>13</sup>, S. De Ridder<sup>22</sup>, P. Desiati<sup>27</sup>,  
M. de With<sup>9</sup>, T. DeYoung<sup>38</sup>, J. C. Díaz-Vélez<sup>27</sup>, M. Dunkman<sup>38</sup>, R. Eagan<sup>38</sup>,  
B. Eberhardt<sup>28</sup>, J. Eisch<sup>27</sup>, R. W. Ellsworth<sup>16</sup>, S. Euler<sup>1</sup>, P. A. Evenson<sup>31</sup>,  
O. Fadiran<sup>27</sup>, A. R. Fazely<sup>6</sup>, A. Fedynitch<sup>10</sup>, J. Feintzeig<sup>27</sup>, T. Feusels<sup>22</sup>,  
K. Filimonov<sup>7</sup>, C. Finley<sup>34</sup>, T. Fischer-Wasels<sup>40</sup>, S. Flis<sup>34</sup>, A. Franckowiak<sup>11</sup>,  
R. Franke<sup>41</sup>, K. Frantzen<sup>19</sup>, T. Fuchs<sup>19</sup>, T. K. Gaisser<sup>31</sup>, J. Gallagher<sup>26</sup>,  
L. Gerhardt<sup>8,7</sup>, L. Gladstone<sup>27</sup>, T. Glüsenkamp<sup>41</sup>, A. Goldschmidt<sup>8</sup>,  
G. Golup<sup>13</sup>, J. A. Goodman<sup>16</sup>, D. Góra<sup>41</sup>, D. Grant<sup>20</sup>, A. Groß<sup>30</sup>,  
M. Gurtner<sup>40</sup>, C. Ha<sup>8,7</sup>, A. Haj Ismail<sup>22</sup>, P. Hallen<sup>1</sup>, A. Hallgren<sup>39</sup>,  
F. Halzen<sup>27</sup>, K. Hanson<sup>12</sup>, D. Heereman<sup>42</sup>, P. Heimann<sup>1</sup>, D. Heinen<sup>1</sup>,  
K. Helbing<sup>40</sup>, R. Hellauer<sup>16</sup>, S. Hickford<sup>15</sup>, G. C. Hill<sup>2</sup>, K. D. Hoffman<sup>16</sup>,  
R. Hoffmann<sup>40</sup>, A. Homeier<sup>11</sup>, K. Hoshina<sup>27</sup>, W. Huelsnitz<sup>16,2</sup>, P. O. Hulth<sup>34</sup>,  
K. Hultqvist<sup>34</sup>, S. Hussain<sup>31</sup>, A. Ishihara<sup>14</sup>, E. Jacobi<sup>41</sup>, J. Jacobsen<sup>27</sup>,  
K. Jagielski<sup>1</sup>, G. S. Japaridze<sup>4</sup>, K. Jero<sup>27</sup>, O. Jlelati<sup>22</sup>, B. Kaminsky<sup>41</sup>,  
A. Kappes<sup>9</sup>, T. Karg<sup>41</sup>, A. Karle<sup>27</sup>, J. L. Kelley<sup>27</sup>, J. Kiryluk<sup>35</sup>, F. Kislak<sup>41</sup>,  
J. Kläs<sup>40</sup>, S. R. Klein<sup>8,7</sup>, J.-H. Köhne<sup>19</sup>, G. Kohnen<sup>29</sup>, H. Kolanoski<sup>9</sup>,  
L. Köpke<sup>28</sup>, C. Kopper<sup>27</sup>, S. Kopper<sup>40</sup>, D. J. Koskinen<sup>38</sup>, M. Kowalski<sup>11</sup>,  
M. Krasberg<sup>27</sup>, K. Krings<sup>1</sup>, G. Kroll<sup>28</sup>, J. Kunnen<sup>13</sup>, N. Kurahashi<sup>27</sup>,  
T. Kuwabara<sup>31</sup>, M. Labare<sup>13</sup>, H. Landsman<sup>27</sup>, M. J. Larson<sup>36</sup>,  
M. Lesiak-Bzdak<sup>35</sup>, M. Leuermann<sup>1</sup>, J. Leute<sup>30</sup>, J. Lünemann<sup>28</sup>, J. Madsen<sup>33</sup>,  
R. Maruyama<sup>27</sup>, K. Mase<sup>14</sup>, H. S. Matis<sup>8</sup>, F. McNally<sup>27</sup>, K. Meagher<sup>16</sup>,  
M. Merck<sup>27</sup>, P. Mészáros<sup>37,38</sup>, T. Meures<sup>12</sup>, S. Miarecki<sup>8,7</sup>, E. Middell<sup>41</sup>,

\*Corresponding author. Email: wellons@icecube.wisc.edu, Phone: 304-542-4464, Address: Wisconsin Institutes for Discovery, 330 N. Orchard St., Madison, WI 53715

<sup>1</sup>Physics Department, South Dakota School of Mines and Technology, Rapid City, SD 57701, USA

<sup>2</sup>Los Alamos National Laboratory, Los Alamos, NM 87545, USA

<sup>3</sup>also Sezione INFN, Dipartimento di Fisica, I-70126, Bari, Italy

<sup>4</sup>NASA Goddard Space Flight Center, Greenbelt, MD 20771, USA

37 N. Milke<sup>19</sup>, J. Miller<sup>13</sup>, L. Mohrmann<sup>41</sup>, T. Montaruli<sup>21,3</sup>, R. Morse<sup>27</sup>,  
 38 R. Nahnhauser<sup>41</sup>, U. Naumann<sup>40</sup>, H. Niederhausen<sup>35</sup>, S. C. Nowicki<sup>20</sup>,  
 39 D. R. Nygren<sup>8</sup>, A. Obertacke<sup>40</sup>, S. Odrowski<sup>30</sup>, A. Olivas<sup>16</sup>, M. Olivo<sup>10</sup>,  
 40 A. O’Murchadha<sup>12</sup>, L. Paul<sup>1</sup>, J. A. Pepper<sup>36</sup>, C. Pérez de los Heros<sup>39</sup>,  
 41 C. Pfendner<sup>17</sup>, D. Pieloth<sup>19</sup>, N. Pirk<sup>41</sup>, J. Posselt<sup>40</sup>, P. B. Price<sup>7</sup>,  
 42 G. T. Przybylski<sup>8</sup>, L. Rädcl<sup>1</sup>, K. Rawlins<sup>3</sup>, P. Redl<sup>16</sup>, R. Reimann<sup>1</sup>,  
 43 E. Resconi<sup>30</sup>, W. Rhode<sup>19</sup>, M. Ribordy<sup>24</sup>, M. Richman<sup>16</sup>, B. Riedel<sup>27</sup>,  
 44 J. P. Rodrigues<sup>27</sup>, C. Rott<sup>17</sup>, T. Ruhe<sup>19</sup>, B. Ruzybayev<sup>31</sup>, D. Ryckbosch<sup>22</sup>,  
 45 S. M. Saba<sup>10</sup>, T. Salameh<sup>38</sup>, H.-G. Sander<sup>28</sup>, M. Santander<sup>27</sup>, S. Sarkar<sup>32</sup>,  
 46 K. Schatto<sup>28</sup>, M. Scheel<sup>1</sup>, F. Scheriau<sup>19</sup>, T. Schmidt<sup>16</sup>, M. Schmitz<sup>19</sup>,  
 47 S. Schoenen<sup>1</sup>, S. Schöneberg<sup>10</sup>, L. Schönherr<sup>1</sup>, A. Schönwald<sup>41</sup>, A. Schukraft<sup>1</sup>,  
 48 L. Schulte<sup>11</sup>, O. Schulz<sup>30</sup>, D. Seckel<sup>31</sup>, S. H. Seo<sup>34</sup>, Y. Sestayo<sup>30</sup>,  
 49 S. Seunarine<sup>33</sup>, C. Sheremata<sup>20</sup>, M. W. E. Smith<sup>38</sup>, M. Soiron<sup>1</sup>, D. Soldin<sup>40</sup>,  
 50 G. M. Spiczak<sup>33</sup>, C. Spiering<sup>41</sup>, M. Stamatikos<sup>17,4</sup>, T. Stanev<sup>31</sup>, A. Stasik<sup>11</sup>,  
 51 T. Stezelberger<sup>8</sup>, R. G. Stokstad<sup>8</sup>, A. Stöbl<sup>41</sup>, E. A. Strahler<sup>13</sup>, R. Ström<sup>39</sup>,  
 52 G. W. Sullivan<sup>16</sup>, H. Taavola<sup>39</sup>, I. Taboada<sup>5</sup>, A. Tamburro<sup>31</sup>,  
 53 S. Ter-Antonyan<sup>6</sup>, S. Tilav<sup>31</sup>, P. A. Toale<sup>36</sup>, S. Toscano<sup>27</sup>, M. Usner<sup>11</sup>,  
 54 D. van der Drift<sup>8,7</sup>, N. van Eijndhoven<sup>13</sup>, A. Van Overloop<sup>22</sup>, J. van Santen<sup>27</sup>,  
 55 M. Vehringer<sup>1</sup>, M. Voge<sup>11</sup>, M. Vraeghe<sup>22</sup>, C. Walck<sup>34</sup>, T. Waldenmaier<sup>9</sup>,  
 56 M. Wallraff<sup>1</sup>, R. Wasserman<sup>38</sup>, Ch. Weaver<sup>27</sup>, M. Wellons<sup>27,\*</sup>, C. Wendt<sup>27</sup>,  
 57 S. Westerhoff<sup>27</sup>, N. Whitehorn<sup>27</sup>, K. Wiebe<sup>28</sup>, C. H. Wiebusch<sup>1</sup>,  
 58 D. R. Williams<sup>36</sup>, H. Wissing<sup>16</sup>, M. Wolf<sup>34</sup>, T. R. Wood<sup>20</sup>, K. Woschnagg<sup>7</sup>,  
 59 C. Xu<sup>31</sup>, D. L. Xu<sup>36</sup>, X. W. Xu<sup>6</sup>, J. P. Yanez<sup>41</sup>, G. Yodh<sup>23</sup>, S. Yoshida<sup>14</sup>,  
 60 P. Zarzhitsky<sup>36</sup>, J. Ziemann<sup>19</sup>, S. Zierke<sup>1</sup>, A. Zilles<sup>1</sup>, M. Zoll<sup>34</sup>, B. Recht<sup>42</sup>,  
 61 C. Ré<sup>42</sup>

62 <sup>1</sup>III. Physikalisches Institut, RWTH Aachen University, D-52056 Aachen, Germany

63 <sup>2</sup>School of Chemistry & Physics, University of Adelaide, Adelaide SA, 5005 Australia

64 <sup>3</sup>Dept. of Physics and Astronomy, University of Alaska Anchorage, 3211 Providence Dr.,  
 65 Anchorage, AK 99508, USA

66 <sup>4</sup>CTSPS, Clark-Atlanta University, Atlanta, GA 30314, USA

67 <sup>5</sup>School of Physics and Center for Relativistic Astrophysics, Georgia Institute of  
 68 Technology, Atlanta, GA 30332, USA

69 <sup>6</sup>Dept. of Physics, Southern University, Baton Rouge, LA 70813, USA

70 <sup>7</sup>Dept. of Physics, University of California, Berkeley, CA 94720, USA

71 <sup>8</sup>Lawrence Berkeley National Laboratory, Berkeley, CA 94720, USA

72 <sup>9</sup>Institut für Physik, Humboldt-Universität zu Berlin, D-12489 Berlin, Germany

73 <sup>10</sup>Fakultät für Physik & Astronomie, Ruhr-Universität Bochum, D-44780 Bochum,  
 74 Germany

75 <sup>11</sup>Physikalisches Institut, Universität Bonn, Nussallee 12, D-53115 Bonn, Germany

76 <sup>12</sup>Université Libre de Bruxelles, Science Faculty CP230, B-1050 Brussels, Belgium

77 <sup>13</sup>Vrije Universiteit Brussel, Dienst ELEM, B-1050 Brussels, Belgium

78 <sup>14</sup>Dept. of Physics, Chiba University, Chiba 263-8522, Japan

79 <sup>15</sup>Dept. of Physics and Astronomy, University of Canterbury, Private Bag 4800,  
 80 Christchurch, New Zealand

81 <sup>16</sup>Dept. of Physics, University of Maryland, College Park, MD 20742, USA

82 <sup>17</sup>Dept. of Physics and Center for Cosmology and Astro-Particle Physics, Ohio State  
 83 University, Columbus, OH 43210, USA

84 <sup>18</sup>Dept. of Astronomy, Ohio State University, Columbus, OH 43210, USA

85 <sup>19</sup>Dept. of Physics, TU Dortmund University, D-44221 Dortmund, Germany

86 <sup>20</sup>Dept. of Physics, University of Alberta, Edmonton, Alberta, Canada T6G 2E1

- 87 <sup>21</sup>*Département de physique nucléaire et corpusculaire, Université de Genève, CH-1211*  
88 *Genève, Switzerland*
- 89 <sup>22</sup>*Dept. of Physics and Astronomy, University of Gent, B-9000 Gent, Belgium*
- 90 <sup>23</sup>*Dept. of Physics and Astronomy, University of California, Irvine, CA 92697, USA*
- 91 <sup>24</sup>*Laboratory for High Energy Physics, École Polytechnique Fédérale, CH-1015 Lausanne,*  
92 *Switzerland*
- 93 <sup>25</sup>*Dept. of Physics and Astronomy, University of Kansas, Lawrence, KS 66045, USA*
- 94 <sup>26</sup>*Dept. of Astronomy, University of Wisconsin, Madison, WI 53706, USA*
- 95 <sup>27</sup>*Dept. of Physics and Wisconsin IceCube Particle Astrophysics Center, University of*  
96 *Wisconsin, Madison, WI 53706, USA*
- 97 <sup>28</sup>*Institute of Physics, University of Mainz, Staudinger Weg 7, D-55099 Mainz, Germany*
- 98 <sup>29</sup>*Université de Mons, 7000 Mons, Belgium*
- 99 <sup>30</sup>*T.U. Munich, D-85748 Garching, Germany*
- 100 <sup>31</sup>*Bartol Research Institute and Department of Physics and Astronomy, University of*  
101 *Delaware, Newark, DE 19716, USA*
- 102 <sup>32</sup>*Dept. of Physics, University of Oxford, 1 Keble Road, Oxford OX1 3NP, UK*
- 103 <sup>33</sup>*Dept. of Physics, University of Wisconsin, River Falls, WI 54022, USA*
- 104 <sup>34</sup>*Oskar Klein Centre and Dept. of Physics, Stockholm University, SE-10691 Stockholm,*  
105 *Sweden*
- 106 <sup>35</sup>*Department of Physics and Astronomy, Stony Brook University, Stony Brook, NY*  
107 *11794-3800, USA*
- 108 <sup>36</sup>*Dept. of Physics and Astronomy, University of Alabama, Tuscaloosa, AL 35487, USA*
- 109 <sup>37</sup>*Dept. of Astronomy and Astrophysics, Pennsylvania State University, University Park,*  
110 *PA 16802, USA*
- 111 <sup>38</sup>*Dept. of Physics, Pennsylvania State University, University Park, PA 16802, USA*
- 112 <sup>39</sup>*Dept. of Physics and Astronomy, Uppsala University, Box 516, S-75120 Uppsala, Sweden*
- 113 <sup>40</sup>*Dept. of Physics, University of Wuppertal, D-42119 Wuppertal, Germany*
- 114 <sup>41</sup>*DESY, D-15735 Zeuthen, Germany*
- 115 <sup>42</sup>*Dept. of Computer Sciences, University of Wisconsin, Madison, WI 53706, USA*

---

116 **Abstract**

117 The IceCube detector is a high-energy neutrino telescope located at the geo-  
118 graphic South Pole. Neutrinos cannot be directly observed and must be inferred  
119 from their interactions with other particles. These interactions sometimes gener-  
120 ate a muon, which in turn emits observable light. At the energies the IceCube  
121 detector is sensitive to, the neutrino and generated muon have almost parallel  
122 paths, so the neutrino path can be inferred from a reconstruction of the muon  
123 path. However, reconstructing the muon path from the observed light is chal-  
124 lenging due to noise, outliers in the data, and the possibility of simultaneously  
125 multiple muons inside the detector.

126 This manuscript describes our work on two problems: (1) the *path recon-*  
127 *struction* problem, in which, given a set of observations, our goal is to recover  
128 the path of a muon, and (2) the *coincident event* problem, which is to deter-  
129 mine how many muons are active in the detector during a time window. Rather  
130 than solving these problems by developing more complex physical models, our  
131 approach is to augment the detector's current models with simple filters and  
132 robust statistical techniques. Using the metric of median angular resolution,  
133 a standard metric for path reconstruction, our solution improves the accuracy

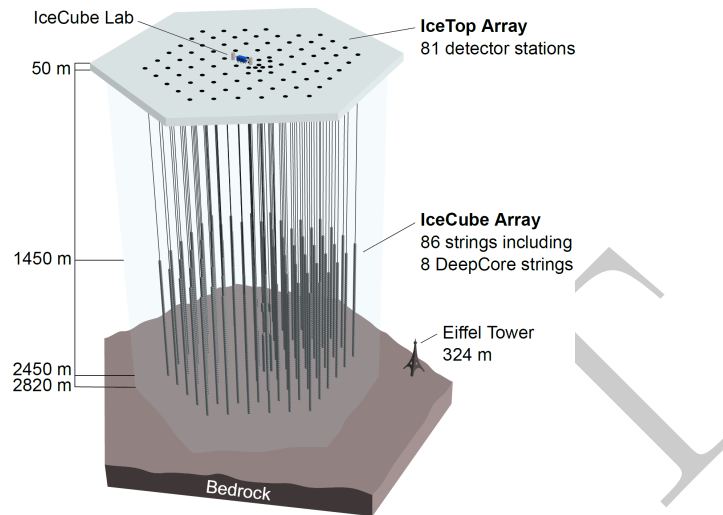


Figure 1: The IceCube neutrino detector in the Antarctic ice. A picture of the Eiffel Tower is shown for scale.

134 in the reconstruction direction by 13%. Our solution for the coincident-event  
 135 problem accurately determines the number of muons 98% of the time, which is  
 136 an improvement of 86% over the software previously used in IceCube.

137 *Keywords:* IceCube, Track reconstruction, Neutrino telescope, Neutrino  
 138 astrophysics, Robust Statistics

---

139 **1. Introduction**

140 The IceCube neutrino detector searches for neutrinos that are generated by  
 141 the universe’s most violent astrophysical events: exploding stars, gamma ray  
 142 bursts, and cataclysmic phenomena involving black holes and neutron stars [1].  
 143 The detector, roughly a cubic kilometer in size, is located near the geographic  
 144 South Pole and is buried to a depth of about 2.5 km in the Antarctic ice [2].  
 145 The detector is illustrated in Figure 1 and a more complete description is given  
 146 in Section 2.

147 We examine two problems that arise in the IceCube detector’s neutrino  
 148 detection:

- 149 1. *Reconstruction*, in which the path of a muon is reconstructed from the  
 150 observed light at different positions and times in the detector.
- 151 2. *Coincident Event Detection*, in which we detect the number of muons  
 152 inside the detector, and assign observed photons to a muon.

153 The IceCube Collaboration has spent considerable effort on both of these  
154 problems over the last decade, as they are a critical step for data analysis.  
155 They have developed sophisticated domain models that take into account the  
156 interaction of near- and far-field effects of light, and have undertaken complex  
157 mapping efforts to understand the effects of photon propagation in the ice [3,  
158 4]. Our solutions do not further refine the detailed modeling of these physical  
159 effects, but instead augment the models with off-the-shelf statistical techniques  
160 combined with some simple data filtering to remove outliers.

161 *Related Work.* Track reconstruction and coincident event detection challenges  
162 are ubiquitous in particle physics [5–7], both in particle accelerators and cosmic  
163 particle detectors. While the work described in this manuscript builds on the  
164 previous technique developed for the IceCube detector [3], our techniques are  
165 general purpose, and potentially have applications in detectors beyond IceCube.

166 *Outline.* We begin by describing the necessary background on the IceCube de-  
167 tector in Section 2. In Section 3, we describe the reconstruction pipeline in-  
168 cluding the prior IceCube software, then we discuss our work and its results.  
169 Section 4 describes our work on coincident event detection, and follows a parallel  
170 structure to Section 3. We describe how in this application, a simple heuristic  
171 approach is an improvement over the prior software. We close with a conclusion  
172 in Section 5.

## 173 2. Background

174 The IceCube detector is composed of 5160 optical detectors, each composed  
175 of a photomultiplier tube (PMT) and onboard digitizer[8]. The PMTs are spread  
176 over 86 vertical strings arranged in a hexagonal shape, with a total instrumented  
177 volume of approximately a cubic kilometer. The PMTs on a given string are sep-  
178 arated vertically by 17 m, and the string-to-string separation is roughly 125 m.

179 When a neutrino enters the telescope, it sometimes interacts with the ice  
180 and generates a muon. As the muon travels through the detector, it radiates  
181 light[9], which is observed by the PMTs and broken down into discrete *hits*[10].  
182 A collection of hits is called an *event*, and if the number of hits in an event is  
183 sufficiently large, the muon path reconstruction algorithm is triggered.

### 184 2.1. Cosmic Ray Background

185 In addition to neutrinos, muons can also be generated by cosmic rays. Ice-  
186 Cube analyses on neutrinos are not interested in cosmic ray muons, and the de-  
187 tector attempts to separate out the cosmic ray muons from the neutrino muons.

188 The primary mechanism for this separation is reconstructing the muon path,  
189 and determining if the muon was traveling downwards into the Earth or upwards  
190 out of the Earth. Since neutrinos can penetrate the Earth but cosmic ray muons  
191 cannot, it follows that a muon traveling out of the Earth must have been caused  
192 by a neutrino. Thus, by selecting only the muons that are reconstructed as  
193 up-going, the cosmic ray muons can, in principle, be removed from the data.

194 *2.2. Challenges in Neutrino Detection*

195 Recovering the muon path from the light measurements is the *reconstruction*  
196 *problem*. The reconstruction algorithms used in the detector have several  
197 challenges which must be overcome. The underlying mechanics are stochastic  
198 and incompletely modeled, the data is noisy and contains outliers, and the  
199 computational abilities of the detector are limited.

200 *Modeling Difficulties.* The underlying physics of the system are nontrivial to  
201 model. The muon's light is scattered by the dust and air crystals in the ice  
202 medium. This scattering is both complex and stochastic, and the scattering  
203 properties of the ice vary with depth [11].

204 *Noise.* An unescapable challenge is the noise inherent in the data. The PMTs  
205 are so sensitive to light that they can record hits even in the absence of nearby  
206 muons. These hits can arise from photons generated either by radioactive decay  
207 inside the PMT or the triboluminescence [12] of the ice.

208 *Computational Constraints.* The reconstruction algorithms are also limited in  
209 complexity by the computing resources available at the South Pole. The path  
210 reconstruction algorithm has to process about 3000 muons per second, so algo-  
211 rithms with excessive computational demands are discouraged.

212 *Cosmic Ray to Neutrino Ratio.* While the cosmic ray muons can in principle  
213 be removed by selecting only muons reconstructed as up-going, the number of  
214 observed cosmic ray muons exceeds the number of observed neutrino muons by  
215 five orders of magnitude [3]. Thus, high accuracy reconstructions are critical  
216 for preventing erroneously reconstructed cosmic ray muons from dominating the  
217 neutrino analysis.

218 **3. Reconstruction Problem**

219 By augmenting the reconstruction algorithm with some simple filters and  
220 classical data analysis techniques, we show significant improvement in the re-  
221 construction algorithm's accuracy.

222 *3.1. Prior IceCube Software*

223 The muon path reconstruction process (outlined in Figure 2) starts when  
224 the number of detected hits exceeds a preset threshold and the data collection  
225 step triggers. After the initial data is collected, it then passes through a series  
226 of simple filters to remove obvious outliers, described more in [13].

227 This is followed by a simple reconstruction algorithm *linefit*, which simply  
228 finds the track that minimizes the sum of the squares of the distances between  
229 the track and the hits. More formally, assume there are  $N$  hits, and denote the  
230 position and time of the  $i$ th hit as  $\vec{x}_i$  and  $t_i$  respectively. Let the reconstructed  
231 muon path have a velocity of  $\vec{v}$ , and let the reconstructed path pass through point

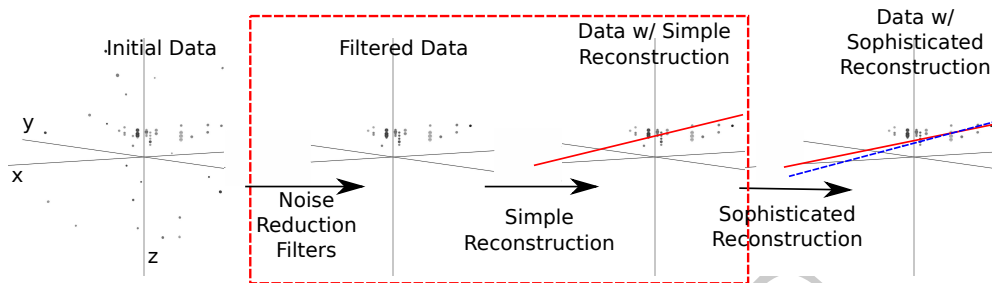


Figure 2: The reconstruction pipeline used to process data in the IceCube detector. After initial data is collected, it is then processed by some simple noise filters, which remove clear outliers. This cleaned data is processed by a simple reconstruction algorithm (red line), which is used as the seed for the more sophisticated reconstruction algorithm (dashed blue line). The sophisticated reconstruction is then evaluated as a potential neutrino. Our work in the reconstruction problem makes changes to the filtering and simple reconstruction step (indicated by the dashed red box).

232  $\vec{x}_0$  at time  $t_0$ . Then linefit reconstruction solves the *least-squares* optimization  
 233 problem

$$\min_{t_0, \vec{x}_0, \vec{v}} \sum_{i=1}^N \rho_i(t_0, \vec{x}_0, \vec{v})^2, \quad (1)$$

234 where

$$\rho_i(t_0, \vec{x}_0, \vec{v}) = \|\vec{v}(t_i - t_0) + \vec{x}_0 - \vec{x}_i\|_2. \quad (2)$$

235 The linefit reconstruction is primarily used to generate an initial track or *seed*  
 236 for a more sophisticated reconstruction.

237 The reconstruction algorithm used in the sophisticated reconstruction *SPE*,  
 238 is described further in [3]. *SPE* takes as input the least-squares reconstruction  
 239 and the event data, and uses a likelihood maximization algorithm to reconstruct  
 240 the muon path.

### 241 3.2. Algorithm Improvement

242 *SPE* is dependent on the seed. Given a seed that is inaccurate by greater than  
 243 or equal to  $6^\circ$ , *SPE* typically cannot recover, and also produces a reconstruction  
 244 inaccurate by greater than or equal to  $6^\circ$ . In addition, the likelihood space for  
 245 *SPE* can contain multiple local maxima, so improving the accuracy of a seed  
 246 already near the true solution still improves the accuracy of *SPE*. Thus, we  
 247 focused our work on improving the quality of the seed.

248 As indicated in Equation 1, a least-squares fit models the muon as a single  
 249 point moving in a straight line, and hits are penalized quadratically in their  
 250 distance from this line. Thus there is an implicit assumption in this model,  
 251 which is that all the hits will be near the muon. There are several pitfalls in  
 252 this assumption:

- 253 1. It ignores the scattering effects of the ice medium. Some of the photons can  
 254 scatter for over a microsecond, which means that when they are recorded  
 255 by a PMT, the muon will be over 300 m away.

256 2. While the noise reduction steps remove most of the outlier noise, the noise  
 257 hits that survive can be far from the muon. Since these outliers are given  
 258 quadratic weight, they exert a huge influence over the model.

259 The first pitfall is a case of the model being incomplete and not modeling  
 260 the data, and the second amounts to the model not being robust to noise. Our  
 261 solution was twofold: improve the model and increase the noise robustness by  
 262 replacing least squares with robust statistical techniques.

### 263 3.2.1. Improving the Model

264 The least-squares model does not model the scattering, and thus hits gen-  
 265 erated by photons that scattered for a significant length of time are not useful  
 266 predictors of the muon’s position. We found that a simple filter could identify  
 267 these scattered hits, and generate an accuracy improvement of almost a factor  
 268 of two by removing them from the dataset.

269 More formally, for each hit  $h_i$ , the algorithm looks at all neighboring hits  
 270 within a neighborhood of  $r$ , and if there exists a neighboring hit  $h_j$  with a time  
 271 stamp that is  $t$  earlier than  $h_i$ , then  $h_i$  is considered a scattered hit, and is not  
 272 used in the simple reconstruction algorithm. Optimal values of  $r$  and  $t$  were  
 273 found to be 156 m and 778 ns by parameter search.

### 274 3.2.2. Adding Robustness to Noise

275 One of the fundamental problems with least squares is that outliers are given  
 276 a quadratic influence, whereas an ideal model would give outliers zero influence.  
 277 Such an ideal model does not exist, but classical statistics has developed models  
 278 where outliers can be marginalized. We experimented replacing the least-squares  
 279 model with a variety of more robust models: a deadzone-linear fit, a one-norm  
 280 fit, and a Huber fit [14].

281 Of the models that we tested, the Huber penalty function gave the greatest  
 282 increase in reconstruction accuracy. More formally, we replace Equation 1 with  
 283 the optimization problem

$$\min_{t_0, \vec{x}_0, \vec{v}} \sum_{i=1}^N \phi(\rho_i(t_0, \vec{x}_0, \vec{v})), \quad (3)$$

284 where the Huber penalty function  $\phi(\rho)$  is defined as

$$\phi(\rho) \equiv \begin{cases} \rho^2 & \text{if } \rho < \mu \\ \mu(2\rho - \mu) & \text{if } \rho \geq \mu \end{cases} . \quad (4)$$

285 Here,  $\rho_i(t_0, \vec{x}, \vec{v})$  is defined in Equation 2 and  $\mu$  is a constant calibrated to the  
 286 data (in our work, the optimal value of  $\mu$  is 153 m).

287 The Huber penalty function has two regimes. In the near-hit regime ( $\rho < \mu$ )  
 288 hits are assumed to be strongly correlated with the muon’s path, and the Huber  
 289 penalty function behaves like least squares, giving these hits quadratic weight.  
 290 In the far-hit regime ( $\rho \geq \mu$ ), hits are given linear weights as they are more  
 291 likely to be noise.



Table 1: Median angular resolution (degrees) for reconstruction improvements. The first line is the accuracy of the prior least-squares model, and the subsequent lines are the accuracy measurements from cumulatively adding improvements into the simple reconstruction algorithm.

Algorithm	$\theta_{med}$
Linefit Reconstruction (Least-Squares)	9.917
With Addition of Logical Filter	5.205
With Addition of Huber Regression	4.672
With Addition of Outlier Removal	4.211

292 In addition to its attractive robustness properties, the Huber fit’s weight  
 293 assignment also has the added benefit that it inherently labels points as outliers  
 294 (those with  $\rho \geq \mu$ ). Thus, once the Huber fit is computed, we can go one step  
 295 farther and simply remove the labeled outliers from the dataset. A better fit is  
 296 then obtained by computing the least-squares fit on the data with the outliers  
 297 removed.

### 298 3.3. Results

299 To measure the improvement generated by our changes, we use the metric of  
 300 *median angular resolution*  $\theta_{med}$ , which is a standard metric used in the collab-  
 301 oration. The angular resolution of a reconstruction is the arc-distance between  
 302 the reconstruction and the true path. Removing the scattered hits and adding  
 303 robustness to the model generates measurable a improvement to the model’s  
 304 accuracy, as shown in Table 1.

305 We can improve the median angular resolution of the simple reconstruction  
 306 by 57.6%. Seeding SPE with the improved simple reconstruction generates an  
 307 improvement in the angular resolution of 12.9%. These improvements in the  
 308 reconstruction algorithm result in 10% fewer atmospheric muons erroneously  
 309 reconstructed as up-going, and 1% more muons correctly reconstructed as up-  
 310 going.

## 311 4. Coincident Event Problem

312 In our second experiment, we look at the problem of determining when more  
 313 than one muon has entered the detector. In the most common case, a single  
 314 muon will pass though the detector and generate an event before exiting. These  
 315 events are processed by the pipeline described in Figure 2. However, for roughly  
 316 9% of the events collected by the data collection algorithm, more than one muon  
 317 will be passing though the detector simultaneously, an occurrence known as a  
 318 *coincident event*.

319 One of the primary sources of background noise in the scientific analyses  
 320 of the IceCube Collaboration is coincident background muons that have been  
 321 erroneously reconstructed as neutrinos. To see why this occurs, consider the  
 322 coincident event shown in Figure 3. There are two clear groups of hits; how-  
 323 ever, the reconstruction algorithm treats them as a single group, resulting in a

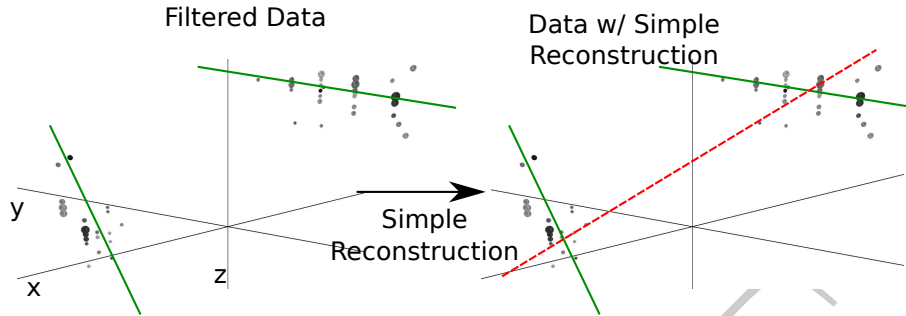


Figure 3: In this example, an event that is clearly composed of two muons (actual tracks shown as green thick lines) is treated as a single muon, and thus the reconstruction (shown in dashed red) is inaccurate.

324 erroneous reconstruction. In the ideal case, the reconstruction algorithm would  
 325 identify coincident events and split them, as in Figure 4.

326 The challenge in this example is determining the number of muons in an  
 327 event. In our results, we find that a simple spatial clustering algorithm can  
 328 solve this classification problem with less than 2% error.

#### 329 4.1. Prior IceCube Software

330 Coincident events have been a concern in the IceCube analysis [15] for years,  
 331 and some software has been developed to handle coincident events. As a baseline  
 332 of comparison, we use the *TTrigger* software, which is described in [16].

#### 333 4.2. Algorithm Improvement

334 Our solution to this problem is a proximal clustering algorithm. The intu-  
 335 ition in proximal clustering is that points local in space and time are probably  
 336 from the same muon. The proximal clustering algorithm iterates through each  
 337 pair of hits  $(i, j)$  and builds an adjacency matrix  $\mathbf{A}$  as

$$\mathbf{A}_{ij} = \begin{cases} 1 & \text{if } \|\Delta x^2 + \Delta y^2 + \Delta z^2 + (c\Delta t)^2\|_2 \leq \alpha, \\ 0 & \text{otherwise} \end{cases} \quad (5)$$

338 where  $\Delta x, \Delta y, \Delta z$  and  $\Delta t$  are the space and time differences between the pair of  
 339 hits, and  $\alpha$  is tuned to the data. The clustering can be recovered by extracting  
 340 the connected components of the graph defined by  $\mathbf{A}$ .

##### 341 4.2.1. Improving the Model

342 When implemented naively, proximal clustering succeeded for the majority  
 343 of the events, but failed if there was a gap in the muon track, which can occur  
 344 when the muon travels through dusty ice. If there is a significantly large gap,  
 345 the algorithm erroneously separates the hits into two clusters.

346 To get around this, an additional heuristic is added, *track connecting*. Af-  
 347 ter the data segmentation is finished, track connecting determines if separate

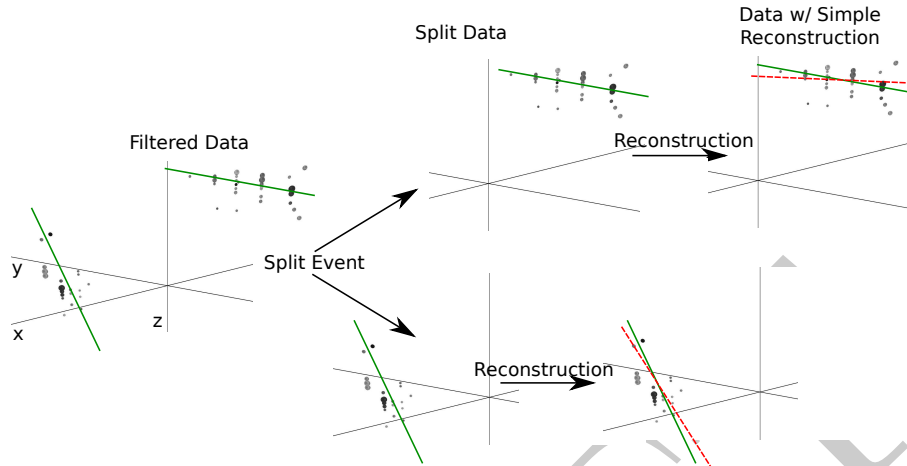


Figure 4: Ideally, the detector would split coincident events before computing the reconstruction. Splitting the event results in more accurate reconstructions (reconstructions shown in red, true muon tracks shown in green). Note the difference in the reconstructions compared with Figure 3.

348 clusters should be combined. It computes the mean position and time of each  
 349 cluster, and connects a hypothetical muon track  $T$  between each pair of sub-  
 350 spaces.

351 It checks if the speed  $s$  of the hypothetical path is within 25% of the speed  
 352 of light  $c$ , and it checks that the mean distance between hits and  $T$  in both  
 353 clusters is less than 60 m. If  $T$  passes both checks, the clusters are combined.

#### 354 4.2.2. Adding Robustness to Noise

355 Proximal clustering is susceptible to noise. Noise hits close to two disjoint  
 356 tracks will be considered adjacent to both tracks, connecting the two tracks in  
 357 the adjacency matrix.

358 One heuristic that worked well at mitigating this problem was to use all the  
 359 hits in building the adjacency matrix. During data collection, some hits are  
 360 marked as coincident, which indicates that both they and a neighboring PMT  
 361 reported a hit. These hits have a high probability of not being noise hits, and  
 362 thus exclusively using them to build the adjacency matrix mitigates the problem  
 363 of erroneously connecting two tracks.

364 After the proximal clustering algorithm has extracted the tracks from the  
 365 adjacency matrix, the hits not used in the construction of the adjacency matrix  
 366 are simply assigned to the closest reconstructed track.

#### 367 4.3. Results

368 There were two competing goals for coincident event detection algorithms:  
 369 the algorithm should be conservative enough that events containing single paths

Table 2: Error Rates for Classification Algorithms

Algorithm	$E_{\text{Single}} \%$	$E_{\text{Multiple}} \%$	$E_{\text{tot}} \%$
Trivial	0.0	100.0	8.3
TTrigger	11.5	31.8	13.2
Proximal clustering	0.2	18.9	1.8

370 are not erroneously split, and aggressive enough that a useful fraction of coin-  
371 cident events are split correctly. Erroneously discarding events containing neu-  
372 trinos is worse than erroneously allowing additional noise into the data pool,  
373 as noise can be eliminated by future filtering of the data pool. Our algorithm  
374 is tuned to keep almost all of the single events correctly unsplit, while still  
375 correctly splitting 80% of the coincident events.

#### 376 4.3.1. Measurements

377 We modified the reconstruction pipeline shown in Figure 2, in between the  
378 noise cleaning and the simple reconstruction, by adding a step for coincident  
379 event detection, as shown in Figure 4. This step takes cleaned data and attempts  
380 to classify the event as a single-track or multiple-track event.

381 We ran each algorithm on two datasets of simulated data. One dataset  
382 comprised single-muon events, and the other dataset comprised multiple-muon  
383 events. In each dataset, we measured the classification error  $E$ , which is the  
384 fraction of events that were misclassified. To get a global measurement, we  
385 compute the *total error*  $E_{\text{tot}}$ , defined as

$$E_{\text{tot}} = w_{\text{Single}} E_{\text{Single}} + w_{\text{Multiple}} E_{\text{Multiple}}. \quad (6)$$

386 For computing  $E_{\text{tot}}$ , we use  $w_{\text{Single}} = 0.917$  and  $w_{\text{Multiple}} = 0.083$ , which is  
387 the frequency in which single-muon and multiple-muon events appear in data  
388 simulating the distribution of events that trigger the reconstruction algorithm.

389 We present our results for the coincident event problem by measuring how  
390 well each algorithm performs at determining the number of subspaces in an  
391 event.

392 There are two natural comparisons for our work: the prior software TTrigger,  
393 as well as the trivial algorithm, which always classifies each event as a single-  
394 track event. Clearly, the latter will always get the single-track events correct,  
395 and always get the multiple-track events wrong. We provide a comparison of  
396 these techniques in Table 2. As shown, our software classifies the number of  
397 muons in the detector 86% better than TTrigger.

## 398 5. Conclusions

399 The challenges in the IceCube detector are complex. Despite this complexity,  
400 we found that we can achieve significant improvement via classical data analysis  
401 algorithms and simple models.

402 We looked at the problem of general reconstruction improvement, and found  
403 that by applying a simple filter to the data and adding some robustness to the  
404 fitting algorithm, we got superior reconstructions in the noisy environments of  
405 the IceCube data. Our reconstruction software runs on-site, and is included in  
406 all IceCube analysis.

407 We also looked at the problem of determining the number of muons in the  
408 detector. We found that proximal clustering, the simplest algorithm that we  
409 tried, was as good as or better than all other tested algorithms. Our proximal  
410 clustering algorithm was an 86% improvement over the current software.

## 411 References

- 412 [1] IceCube Collaboration, IceCube webpage, <http://icecube.wisc.edu/>.
- 413 [2] IceCube Collaboration, First year performance of the IceCube neutrino  
414 telescope, *Astroparticle Physics* 26 (3) (2006) 155–173.
- 415 [3] IceCube Collaboration, Muon Track Reconstruction and Data Selection  
416 Techniques in AMANDA, *Nuclear Instruments and Methods in Physics  
417 Research Section A* 524 (2004) 169–194.
- 418 [4] IceCube Collaboration, Measurement of South Pole ice transparency with  
419 the IceCube LED calibration system IceCube Collaboration, *Nuclear In-  
420 struments and Methods in Physics Research Section A*.
- 421 [5] ATLAS Collaboration, Tracking and vertexing with the ATLAS detector at  
422 the LHC, *Nuclear Instruments and Methods in Physics Research Section A:  
423 Accelerators, Spectrometers, Detectors and Associated Equipment* 650 (1)  
424 (2011) 218–223.
- 425 [6] R. S. Chivukulaa, M. Goldena, E. H. Simmons, Multi-jet physics at hadron  
426 colliders, *Nuclear Physics B* 363 (1) (1991) 83–96.
- 427 [7] S. Ellis, J. Huston, K. Hatakeyama, P. Loch, M. Tönnesmann, Jets in  
428 hadron–hadron collisions, *Progress in Particle and Nuclear Physics* (60)  
429 (2008) 484–551.
- 430 [8] IceCube Collaboration, Calibration and characterization of the IceCube  
431 photomultiplier tube, *Nuclear Instruments and Methods in Physics Re-  
432 search Section A* 618 (2010) 139–152.
- 433 [9] IceCube Collaboration, An improved method for measuring muon energy  
434 using the truncated mean of  $dE/dx$ , *Nuclear Instruments and Methods in  
435 Physics Research Section A*.
- 436 [10] IceCube Collaboration, The icecube data acquisition system: Signal cap-  
437 ture, digitization, and timestamping, *Nuclear Instruments and Methods in  
438 Physics Research Section A* 601 (3) (2009) 294–316.

- 439 [11] M. Wolf, E. Resconi, Verification of South Pole glacial ice simulations in Ice-  
440 Cube and its relation to conventional and new, accelerated photon tracking  
441 techniques, Master's thesis, Max-Planck-Institut für Kernphysik Heidelberg  
442 (September 2010).
- 443 [12] IceCube Collaboration, IceCube sensitivity for low-energy neutrinos from  
444 nearby supernovae, *Astronomy & Astrophysics* 535 (A109) (2011) 18.
- 445 [13] M. Ackermann, Searches for signals from cosmic point-like sources of high  
446 energy neutrinos in 5 years of AMANDA-II data, Ph.D. thesis, Humboldt-  
447 Universität zu Berlin (2006).
- 448 [14] S. Boyd, L. Vandenberghe, *Convex Optimization*, Cambridge University  
449 Press, 2009.
- 450 [15] IceCube Collaboration, Measurement of the atmospheric neutrino energy  
451 spectrum from 100 GeV to 400 TeV with IceCube, *Physical Review D*  
452 83 (1).
- 453 [16] D. Chirkin, Measurement of the atmospheric neutrino energy spectrum  
454 with IceCube, Proceedings of the 31st ICRC.